Shieldless Eddy-Current Displacement Sensor with Improved Measurement Sensitivity

Vogel, Johan G.; Chaturvedi, Vikram; Nihtianov, Stoyan

DOI
10.1109/ET.2018.8549631

Publication date
2018

Document Version
Final published version

Published in
2018 IEEE 27th International Scientific Conference Electronics, ET 2018 - Proceedings

Shieldless Eddy-Current Displacement Sensor with Improved Measurement Sensitivity

Johan G. Vogel, Vikram Chaturvedi and Stoyan Nihtianov
Electronic Instrumentation Laboratory
Delft University of Technology
Mekelweg 4, 2628CD Delft, The Netherlands
j.g.vogel@tudelft.nl

Abstract – **The major limitations of eddy-current displacement sensors, such as low measurement sensitivity and low stability, can be mitigated by using low-inductance flat coils in combination with a ratiometric measurement and a high excitation frequency, thus making eddy-current sensors of interest for high-precision applications. For the ratiometric measurement, the sensing coil is used in combination with a constant inductance reference coil, which are magnetically isolated from each other by a shield. In this paper, the implications of omitting the shield are studied. It is shown that a shieldless design brings several advantages related to sensitivity, compactness and manufacturability.**

Keywords – **eddy-current sensor, displacement sensing, ratiometric measurement, sensor design, magnetic shielding**

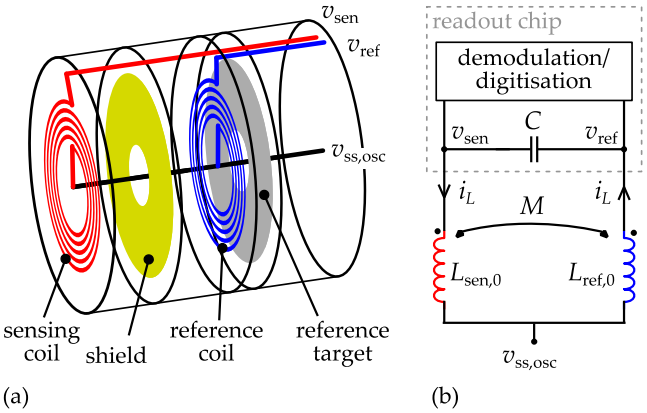

Fig. 1. (a) Coil stack of the high-precision eddy-current displacement sensor. (b) Circuit diagram of the oscillator.

I. Introduction

In many high-precision applications, such as lithography machines and space equipment, displacement measurement with nanometre resolution is required [1]. Various types of displacement sensors are available for this purpose, each with its own advantages and limitations [2].

Capacitive displacement sensors are often used in high-precision applications due to their high resolution, relatively low cost and small built-in volume. However, capacitive sensors are sensitive to environmental parameters, such as humidity [3].

Eddy-Current Displacement Sensors (ECDSs) have similar properties to capacitive sensors, but they have typically a lower resolution and a lower stability. For this reason, they are not often used in high-precision applications. Still, they are interesting because of their low sensitivity to environmental parameters [4].

The limitations of the industrial ECDSs currently available are related to their operation principle and architecture. State-of-the-art industrial ECDSs make use of large wound coils which are mechanically unstable. Furthermore, they use excitation frequencies of only up to 2 MHz, which leads to a relatively large skin depth for the eddy currents that are induced in the measurement target. This, in turn, leads to a high sensitivity to the temperature of the target [5].

To mitigate the limitations of the present ECDSs, a novel ECDS was developed [6], which uses a much higher excitation frequency between 100 MHz and 200 MHz. This reduces the cross-sensitivity to the temperature of the target and makes it possible to use a flat low-inductance coil that is more mechanically stable. A dedicated low-power readout chip makes it possible to integrate the electronics directly in the sensor probe, thus eliminating long cabling and its inherent distortion and parasitics. The sensor prototype showed a resolution in the order of nanometres at a 2 kHz bandwidth [6].

Based on this prototype, a miniaturised eddy-current probe has been designed [7]. This probe contains the sensing coil (with an inductance $L_{sen,0}$), a reference coil (with an inductance $L_{ref,0}$), a stationary reference target and the readout chip (Fig. 1a). It has been shown that the coils and the reference target can be integrated in a single stack. This allows the sensing coil and the reference coil to be closely spaced, thus decreasing their thermal gradient, so that the effect of thermal expansion is partly cancelled. A compact stack was designed with a diameter of 12 mm and a thickness of 2 mm.

In order to isolate the magnetic field of the sensing coil and the reference coil, an intermediate conductive shield was used. This shield makes the mutual inductance between the coils practically zero, so that the inductance of the reference coil is not affected by the standoff distance between the probe and the measurement target.

A drawback of a shield in the vicinity of the measurement coil is that it leads to sensitivity loss. Thus, a certain minimum spacing is required between the shield and the coils in order to limit this decrease. In [7] a spacing of around 540 µm was selected, which leads to a reduction of the measurement sensitivity by 8 %.

978-1-5386-6692-0/18/$31.00 ©2018 IEEE

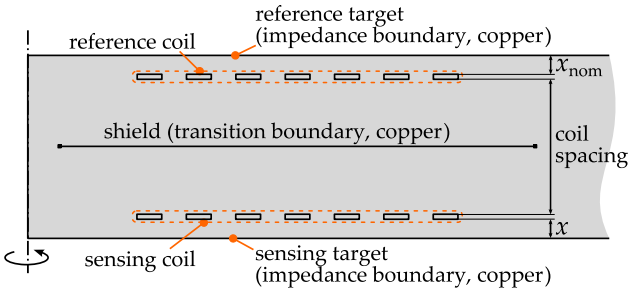

Fig. 2. Axisymmetric FE model of the right-half cross-section of the coil stack with the applied boundary conditions.

However, as the effects of having no shield have not been previously studied, this paper investigates the consequences of omitting the shield. This is done by comparing the measurement sensitivity and compactness of a coil stack with and without a shield. Section II provides the mathematical relations between the ratiometric measurement and the coil inductance. Section III studies the effect of omitting the shield. Section IV studies the influence of coil distance and proposes an optimised shieldless coil stack, which is used for experimental verification.

II. Coil Inductance and Sensitivity

When a shield is applied, the mutual inductance M (Fig. 1b) between the coils is practically zero. In a shieldless configuration, however, it is non-zero. As the coils share the same current i_L, the mutual inductance simply modifies the self-inductance $L_{n,0}$ as follows:

$$L_{\text{sen}} = L_{\text{sen},0} - M \quad \text{and} \quad L_{\text{ref}} = L_{\text{ref},0} - M. \tag{1}$$

The prototype that was realised in [6] generates an output signal that is based on the coil inductances according to the following ratiometric function:

$$D_{\text{out}} = \frac{|v_{\text{sen}}|-|v_{\text{ref}}|}{\beta|v_{\text{ref}}|} \simeq \frac{L_{\text{sen}}-L_{\text{ref}}}{\beta L_{\text{ref}}}, \tag{2}$$

where v_{sen} and v_{ref} are the voltages over the sensing and the reference coil, respectively, and β is a constant that relates the range of the ratio to the range of D_{out}. In this paper, β is chosen equal to 1. As the mutual inductance adds to both L_{sen} and L_{ref}, Eq. (2) can also be written as:

$$D_{\text{out}} \simeq \frac{L_{\text{sen},0} - L_{\text{ref},0}}{\beta L_{\text{ref}}}. \tag{3}$$

The measurement sensitivity in terms of D_{out} is:

$$\frac{\partial D_{\text{out}}}{\partial x} \simeq \frac{\frac{\partial L_{\text{sen},0}}{\partial x} - \frac{\partial L_{\text{ref},0}}{\partial x}}{\beta L_{\text{ref}}} - \frac{L_{\text{sen},0} - L_{\text{ref},0}}{\beta L_{\text{ref}}} \frac{\partial L_{\text{ref}}}{\partial x}. \tag{4}$$

Note that the second term is relatively weak, as both $L_{\text{sen},0} - L_{\text{ref},0}$ and $\partial L_{\text{ref}}/\partial x$ are small.

III. Effect of Omitting the Shield

A. Finite element model

To study the effect of the presence or absence of the intermediate shield, a Finite Element (FE) model was developed using the magnetic fields toolbox in Comsol. As the skin depth at 200 MHz is small (~6 µm in copper) and as the aspect ratios of the coil geometry are large, a 2D axisymmetric model was used. Figure 2 shows the geometry and boundary conditions used in the model. The shield is modelled as a transition boundary which behaves physically as a volume with thickness, but has a geometric thickness of zero. The absence of the shield was modelled by setting its thickness to 1 nm, which is much smaller than the skin depth.

The coils are made of copper, have seven turns, a nominal outer radius (i.e. average radius of the outer turn) of 2.2 mm and a trace width and trace spacing of 0.13 mm.

The presence or absence of the shield and the current direction of the sensing coil with respect to the reference coil were varied, leading to in total four configurations.

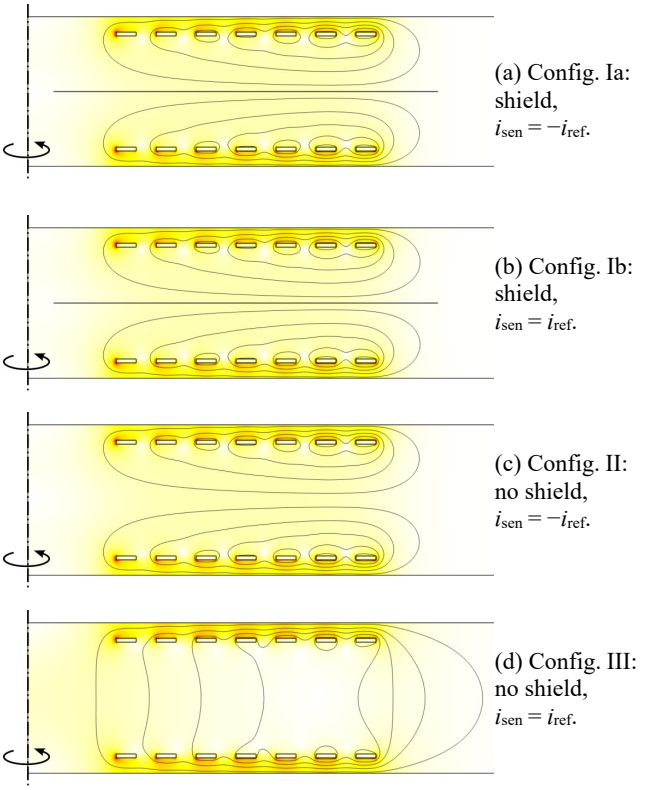

Fig. 3. Magnetic field intensity (colour) and field lines in the right half of the cross-section of the coil stack in four configurations.

B. Magnetic fields

Figure 3 shows the magnetic field intensity and the field lines of the magnetic field for each of the configurations.

In the Configs. Ia and Ib (Fig. 3a and Fig. 3b), the current direction in the coils is opposite and equal, respectively. The shield, however, blocks the magnetic field so that the situation, in terms of magnetic field intensity, is equal.

In Config. II (Fig. 3c) the shield is omitted. The resulting distribution of the magnetic field is very similar to the configurations with a shield, however. This can be explained by the fact that a shield with infinite conductivity acts as a mirror plane, introducing a virtual mirror coil that carries the opposite current, which is similar to Config. II.

In Config. III (Fig. 3d) the shield is omitted and the two coils carry current in the same direction. This leads to a very different distribution of the magnetic field compared to the other configurations.

TABLE 1. INDUCTANCE OF FOUR COIL STACK CONFIGURATIONS.

Configuration	Ia	Ib	II	III
Shield	yes	yes	no	no
Current direction	$i_{sen} = -i_{ref}$	$i_{sen} = i_{ref}$	$i_{sen} = -i_{ref}$	$i_{sen} = i_{ref}$
Self-inductance $L_{n,0}$ [nH]	26.4	26.4	28.9	28.9
Mutual inductance M [nH]	0.0	0.0	2.5	−2.5
Inductance L_n [nH]	26.4	26.4	26.4	31.4
$\partial L_{sen,0}/\partial x$ [nH/µm]	0.158	0.158	0.195	0.195
$\partial L_{ref,0}/\partial x$ [nH/µm]	0.0	0.0	0.002	0.002
$\partial M/\partial x$ [nH/µm]	0.0	0.0	0.019	−0.019
$\partial L_{sen}/\partial x$ [nH/µm]	0.158	0.158	0.176	0.214
$\partial L_{ref}/\partial x$ [nH/µm]	0.0	0.0	−0.017	0.021
Sensitivity $\partial D_{out}/\partial x$ [1/mm]	6.0	6.0	7.4	6.1

** Freq. 200 MHz, nominal standoff 100 µm, coil spacing 720 µm.*

Table 1 provides quantitative results for the four configurations. All values are based on a nominal standoff of 100 µm and a coil spacing of 720 µm.

The results for the two configurations with a shield are equal, as the shield prevents interaction between the coils, so that their relative current direction has no influence.

The coils in Config. II have a slightly higher self-inductance $L_{n,0}$. Owing to the mutual inductance M, their inductance L_n decreases and becomes similar to that in Configs. Ia and Ib. As the shield is removed, the sensitivity of the self-inductance of the measurement coil $\partial L_{sen,0}/\partial x$ increases. Also, the reference coil becomes slightly sensitive ($\partial L_{ref,0}/\partial x$) to standoff change, as well as the mutual inductance ($\partial M/\partial x$).

In Config. III, the self-inductance $L_{n,0}$ of the coils equals that in Config. II. As the mutual inductance M is negative, the inductance L_n becomes higher. The sensitivities of the self-inductance to standoff change $\partial L_{n,0}/\partial x$ are equal to those in Config. II.

Configuration II has a higher measurement sensitivity $\partial D_{out}/\partial x$ compared to Configs. Ia and Ib. This is caused by the higher relative sensitivity of the coils $\partial L_{sen,0}/\partial x - \partial L_{ref,0}/\partial x$, which is a direct result of omitting the shield. Configuration III has the same high relative sensitivity but the measurement sensitivity is only slightly higher than that found in Configs. Ia and Ib, due to its higher inductance.

Of the four configurations, the shieldless configuration with opposing current (Config. II) is the best choice, since it has the highest measurement sensitivity.

IV. OPTIMISED COIL SPACING

A. Influence of coil spacing

To optimise the spacing between the coils, the influence of the spacing on the measurement sensitivity was investigated. This was done using the FE model. Figure 4a shows the inductance as a function of the coil spacing. The coil inductance converges when spacing increases to a common value, regardless of the presence of a shield. In Configs. I and II, the inductance decreases with smaller spacing; in Config. III, it increases due to the positive contribution of the mutual inductance.

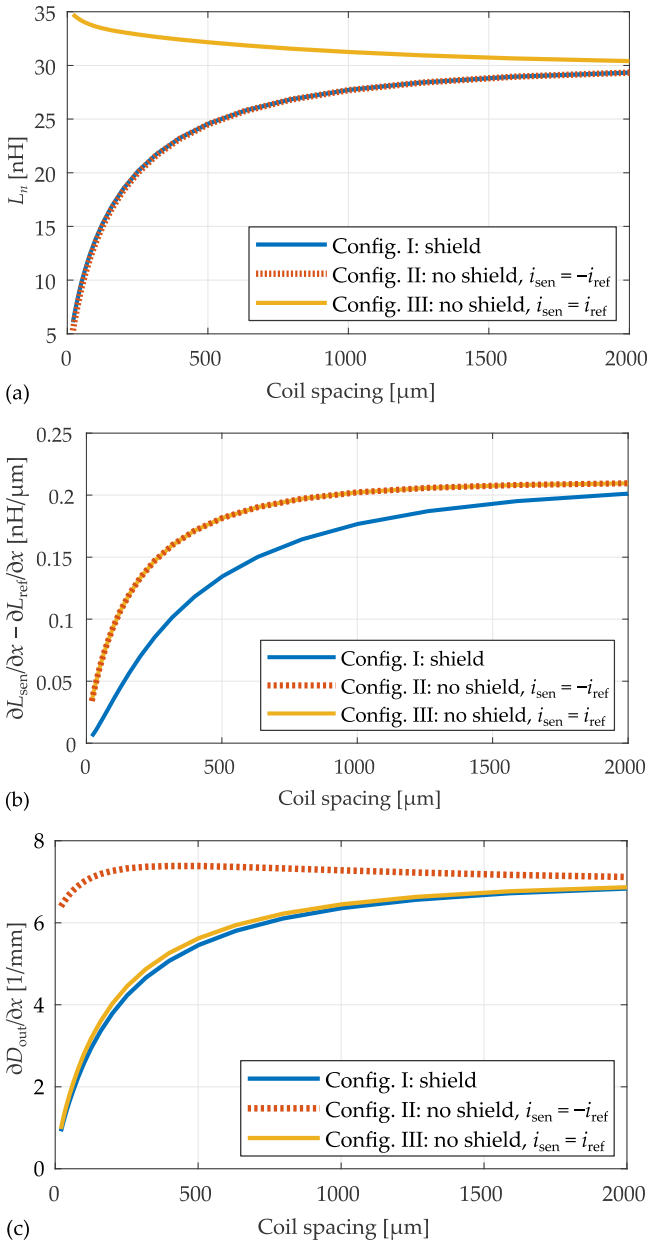

Fig. 4. (a) Inductance of the sensing and reference coils, (b) inductance sensitivity and (c) measurement sensitivity as a function of the coil spacing.

In Fig. 4b the difference between the inductance sensitivities $\partial L_{sen}/\partial x - \partial L_{ref}/\partial x$ is shown. Configurations II and III have equal sensitivity. Configuration I has a lower sensitivity for any value of the spacing.

Figure 4c shows the resulting measurement sensitivity $\partial D_{out}/\partial x$. With large spacing, it converges to the same value in all configurations. The measurement sensitivity of Configs. I and III decrease with decreased spacing, whereas that of Config. II stays more or less constant, even with small spacing (~100 µm), and attains an optimum around a 400 µm spacing.

B. Realised prototypes

The coil stack in Config. II with a spacing of 400 µm attains maximum measurement sensitivity. This stack was manufactured, along with other three eddy-current stack

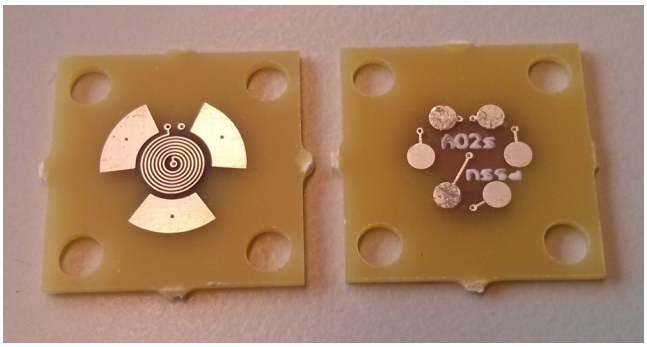

Fig. 5. Coil stack prototype fabricated with multilayer PCB technology.

configurations. The stacks were manufactured using a standard multilayer PCB process. The coil current in the opposite direction ($i_{sen} = -i_{ref}$) was realised by using a reference coil with the same geometry as the sensing coil, whereas the current in the same direction ($i_{sen} = i_{ref}$) was realised by using a mirrored version of the sensing coil as a reference coil.

Figure 5 shows one of the coil stack prototypes that was fabricated.

C. Experimental results

Measurements of the coil stack prototypes were performed using an HP 4294A impedance analyser with a 42941A impedance probe. A frequency of 110 MHz was used—the highest frequency supported by the impedance analyser. The inductances of the sensing coil, the reference coil and the two coils in series were measured to obtain $L_{sen,0}$, $L_{ref,0}$ and $L_{sen} + L_{ref}$, respectively. From these values, L_{sen} and L_{ref} were calculated using Eq. (1). A motorised linear stage was used to vary the standoff of the sensing target. In this way, it was also possible to obtain the derivatives $\partial L_{sen}/\partial x$ and $\partial L_{ref}/\partial x$.

Table 2 lists the measurement results along with results obtained using the FE model. The inductance of the reference coil is close to that of the model. The inductance of the sensing coil in all measurements is higher (around 4 nH) than that of the reference coil. This is probably caused by the longer wiring to the sensing coil, which leads to increased inductance.

In most cases, the sensitivity of the sensing coil, $\partial L_{sen}/\partial x$, in the measurements is lower than that in the model. Together with the somewhat higher inductance L_{ref}, the measurement sensitivity obtained from the measurements is smaller compared to that of the model. The measurements clearly show that the measurement sensitivities of Configs. Ia, Ib and III are close, whereas the sensitivity of Config. II is much higher (i.e. roughly 50 %).

TABLE 2. MEASUREMENT AND MODEL RESULTS OF THE OPTIMISED STACKS.

Configuration	Ia	Ib	II	III
Shield	yes	yes	no	no
Current direction	$i_{sen} = -i_{ref}$	$i_{sen} = i_{ref}$	$i_{sen} = -i_{ref}$	$i_{sen} = i_{ref}$
Inductance L_{sen} [nH]	28.6	30.3	29.7	41.2
Inductance L_{ref} [nH]	26.3	27.3	25.5	35.8
Inductance L_n [nH] (FEM)	23.6	23.6	23.5	32.9
$\partial L_{sen}/\partial x$ [$^{nH}/_{\mu m}$]	0.1063	0.095	0.144	0.202
$\partial L_{ref}/\partial x$ [$^{nH}/_{\mu m}$]	−0.003	−0.008	−0.024	0.041
$\partial L_{sen}/\partial x$ [$^{nH}/_{\mu m}$] (FEM)	0.118	0.118	0.144	0.211
$\partial L_{ref}/\partial x$ [$^{nH}/_{\mu m}$] (FEM)	0.0	0.0	−0.027	0.040
$\partial D_{out}/\partial x$ [$^{1}/_{mm}$]	4.1	3.8	6.7	4.3
$\partial D_{out}/\partial x$ [$^{1}/_{mm}$] (FEM)	5.0	5.0	7.3	5.2

** Freq. 110 MHz, nominal standoff 100 µm, coil spacing 400 µm.*

V. CONCLUSIONS

In eddy-current sensors with a flat sensing coil, a similar reference coil and a ratiometric readout, a shield can be used to magnetically isolate the coils. This paper shows that ommitting this shield offers a number of practical advantages.

By constructing the coils such that they carry current in the opposite direction, the resulting magnetic field is very similar to the situation with a shield, leading to similar coil inductance but higher sensitivity.

In the shielded configuration, the sensitivity drops significantly for smaller coil spacing, whereas in the shieldless configuration, the sensitivity is relatively independent of coil spacing. This allows the coils to be closely spaced in the shieldless configuration, enabling a more compact design and a decrease in the thermal gradients between the coils. For the studied geometry, the shieldless configuration leads, at a coil spacing of only 400 µm, to 46 % higher sensitivity than the shielded configuration; with a much larger 2000 µm coil spacing it still leads to 8 % higher sensitivity.

Finally, ommitting the shield also allows for a simpler and therefore more cost-effective PCB design.

In this study, parasitic capacitive effects were not taken into account. These need to be included in further design stages, where they might impose a lower bound to the allowable coil spacing.

REFERENCES

[1] R. H. Munnig Schmidt, *Ultra-precision engineering in lithographic exposure equipment for the semiconductor industry*, Philosophical Transactions of the RSL A: Mathematical, Physical and Engineering Sciences, vol. 370, no. 1973, pp. 3950–72, 2012.

[2] A. J. Fleming, *A review of nanometer resolution position sensors: Operation and performance*, Sensors and Actuators A: Physical, vol. 190, pp. 106–126, 2013.

[3] S. Nihtianov, *Measuring in the subnanometer range: Capacitive and eddy current nanodisplacement sensors*, IEEE IEM, vol. 8, no. 1, pp. 6–15, Mar. 2014.

[4] B. George, Z. Tan, S. Nihtianov, *Advances in capacitive, eddy current, and magnetic displacement sensors and corresponding interfaces*, IEEE Transactions on Industrial Electronics, vol. 64, no. 12, pp. 9595–9607, Dec. 2017.

[5] V. Chaturvedi, J. G. Vogel, K. A. A. Makinwa, S. Nihtianov, *A 19.8-mW eddy-current displacement sensor interface with sub-nanometer resolution*, IEEE Journal of Solid-State Circuits, accepted for publication, 2018.

[6] V. Chaturvedi, J. G. Vogel, K. A. A. Makinwa, S. Nihtianov, *A 9.1 mW inductive displacement-to-digital converter with 1.85 nm resolution*, in 2017 Symposium on VLSI Circuits, 2017, pp. C80–C81.

[7] J. G. Vogel, V. Chaturvedi, S. Nihtianov, *Probe design for high-precision eddy-current displacement sensors*, in Proceedings of the 44th annual conference of the IEEE Industrial Electronics Society (IECON), 2018.